
Fine-Grained AutoAugmentation for Multi-label Classification

Ya Wang*, Heseng Chen, Fangyi Zhang, Yaohua Wang, Xiuyu Sun,† Ming Lin, Hao Li
Alibaba Group
xiuyu.sxy@alibaba-inc.com

Abstract

Data augmentation is a commonly used approach to improving the generalization of deep learning models. Recent works show that learned data augmentation policies can achieve better generalization than hand-crafted ones. However, most of these works use unified augmentation policies for all samples in a dataset, which is observed not necessarily beneficial for all labels in multi-label classification tasks, i.e., some policies may have negative impacts on some labels while benefitting the others. To tackle this problem, we propose a novel Label-Based AutoAugmentation (LB-Aug) method for multi-label scenarios, where augmentation policies are generated with respect to labels by an augmentation-policy network. The policies are learned via reinforcement learning using policy gradient methods, providing a mapping from instance labels to their optimal augmentation policies. Numerical experiments show that our LB-Aug outperforms previous state-of-the-art augmentation methods by large margins in multiple benchmarks on image and video classification.

1 Introduction

Data augmentation is a powerful technique to enlarge a training dataset with more diversity. For a long time, augmentation policies are manually designed and achieve great success in various tasks, including object recognition [1], image retrieval [2] and video activity recognition [3]. However, the manually designed augmentation policies heavily rely on individual experience and therefore suffer from individual bias. The transfer ability of these policies is also limited. Re-design of augmentation policies is normally required when facing new tasks, which could be time-consuming. To remedy these drawbacks, approaches are recently proposed to automatically learn augmentation policies in a data-driven way [4, 5, 6], obtaining remarkable gains over manually designed ones.

However, most of the aforementioned methods are label-agnostic, where augmentation policies are determined regardless of what class a training instance belongs to. This kind of policies are observed problematic in multi-label classification tasks in our study on the effects of augmentation policies on different labels, as shown in Figure 1(a). The study is conducted using 7 augmentation operators (the row coordinates of Figure 1(a)) on Peta, a pedestrian attribute recognition dataset [7]. The values in the table indicate the effects of each single operator on different labels (the column coordinates), with “P”, “N” and “-” represent positive, negative and neutral effects respectively. A positive effect means a model trained with a certain augmentation operator obtains a better mean accuracy (larger than a threshold) in a certain label than that of a model trained without. From Figure 1(a), it is interesting to see that “perspective” is beneficial to the prediction of global “Casual Upper” and “Jacket”, but harmful to “Long Hair” and “No Carrying”. Meanwhile, the accuracy of “Formal Upper” is increased by “randomcrop” but decreased by “scale”. These results indicate that a certain

*This work was completed during Ya Wang’s internship at Alibaba DAMO Academy.

†Corresponding author, E-mail: xiuyu.sxy@alibaba-inc.com.

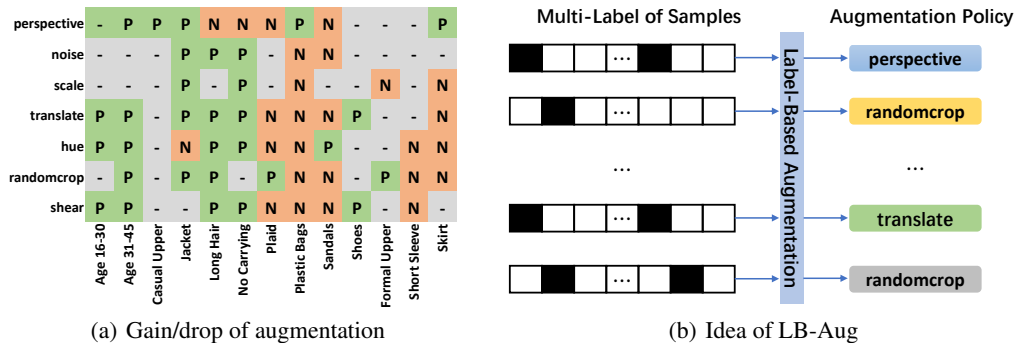


Figure 1: (a) The effects of some exemplary augmentation operators on different labels of Peta, where “P” indicates positive effects on the classification, “N” represents negative effects and “-” means neutral or inconspicuous influences. (b) The idea of LB-Aug: learning policies mapping encoded instance labels to their augmentation policies (probability and settings of each operator).

augmentation operator may have opposite effects on different labels. In other words, label-agnostic policies are not necessarily beneficial to all labels.

To address the above problem, we think instance labels must be considered in a fine-grained manner for data augmentation. To this end, a novel Label-Based AutoAugmentation (LB-Aug) method is proposed in this paper to learn label-aware policies (rather than label-agnostic ones), mapping from instance labels to their optimal data augmentation policies, as shown in Figure 1(b). The policies are learned through reinforcement learning using the Policy Gradient method [8], where a policy is defined by the probabilities of applying each augmentation operator and their parameters. The density matching scheme in FAA [5] is also used here to speed up the policy learning process. The superiority of the method is demonstrated in extensive experiments on Peta, MS-COCO and Charades benchmarks. To the best of our knowledge, LB-Aug is the first label-based fine-grained autoaugmentation method for multi-label classification.

The remainder of this work is organized as follows. First, relevant autoaugmentation methods are summarized in Section 2. Then, the LB-Aug method is introduced in Section 3, followed with extensive experiments in Section 4 demonstrating the superiority of the method and showing how each part of the method contributes to the performance gain via ablation study.

2 Related Work

Data augmentation plays an important role in improving the generalization of deep neural networks, especially for the task on small scale dataset. For example, random crop, flip, rotation, scaling, and color transformation have been performed as baseline augmentation methods in various tasks on ImageNet [9], Kinetics [10] and Charades [3]. Recently, plenty of augmentation methods have been proposed, such as Cutout [11] and Mixed-Example[12]. Though the augmentation policy is a key technique to enhance the generalization of deep neural networks, it is shown that different augmentation operations not always benefit their performance in different tasks. Besides, the hyper-parameters, such as mean and std in GaussianBlur, angle in the RandomRotate should also be chosen carefully. Different from common human designed augmentation operations, the methods of automatical augmentation take various augmentation operations to construct a search space and some sub-policies, and then automatically find the best augmentation policies through various learning strategies. AutoAugment [4] introduces a reinforcement learning based search strategy that alternately trained a child model and RNN controller and leverages the performance of baseline DNN obviously. Although it is accelerated by PPO [13] method, the search process requires thousands of GPU hours. To reduce the searching cost, some improvements have been proposed.

Fast AutoAugmentation (FAA) takes Bayesian optimization as optimizer and the density matching as rewards to avoid training the classifier frequently, its training time is reduced remarkably in comparison with AutoAugment [4], which makes it an available method to be complemented in the task on large scale dataset. Adversarial AutoAugment [6] is also a computationally-affordable

solution, which attempts to increase the training loss of a target network through generating adversarial augmentation policies, while the target network can learn more robust features from harder examples to improve the generalization. PBA [14] generates nonstationary augmentation policy schedules instead of a fixed one to accelerate the search for augmentation policies. In summary, previous learned augmentation methods mainly focus on reducing the searching computational complexity rather than improving the performance and exploring new applications. Since they take augmentation operations and magnitudes into the evaluation without other information, all training samples share the same policies during training. It may be not optimal. On the other hands, the best augmentation policies are evaluated in only single-label classification tasks, e.g. CIFAR-10, CIFAR-100 and ImageNet. When transforming them into a multi-label classification tasks, we cannot obtain an expected result, which is shown in the previous experiment. In the next section, we will explain how do we solve these two major problems.

3 Method

Our method provides fine-grained and label-based augmentation policies from a specific search space (Section 3.1) for each image/video. The generic architecture involves two processes: 1) training an actor network with improved density matching (Section 3.2) as illustrated in Figure 2(a). 2) Using the trained actor network to construct the integral label based augmentation policy for each individual instance, shown in Figure 2(b).

3.1 Label Based Search Space

The search space in this paper contains 16 different operations per [4]. Each operation τ requires a probability p of being called, and a magnitude λ with which it is applied. Formally, a label based augmentation policy $\mathcal{O} = (\tau, p, \lambda, y)$ for instance (x, y) is :

$$\mathcal{O}(x; p, \lambda, y) = \begin{cases} \tau(x; \lambda, y) & \text{with probability } p \\ x & \text{with probability } 1 - p \end{cases} \quad (1)$$

Note that, the calling probability p and magnitude λ in Eqn. 1 are both sensitive to the label y , where the ‘‘Label Based’’ derives from. We also discretize the ranges of calling probability into 11 values and magnitude into 10 values with uniform spacing, so that a discrete optimization algorithm (elaborated in Section 3.2) is available to facilitate the policy search phase.

3.2 Label-based Augmentation

From the perspective presented in Figure 1(a), we propose learning a Label Based AutoAugmentation (LB-Aug) to yield fine-grained augmentation for multi-label classification. The term ‘‘fine-grained’’ implies that the policies are adaptive to different samples with their labels.

3.2.1 Training Actor with Improved Density Matching

Density matching [5] is an efficient mechanism to provide the reward of each policy evaluation without any backpropagation for network training. Given a pair of training and validation datasets D_{train} and D_{valid} , for the purpose of facilitating the generalization ability of policies to match the density of D_{train} and augmented D_{valid} , density matching performs this evaluation by measuring the generalization of the classifier pre-trained on one dataset to the other dataset. In detail, it splits D_{train} into two segments D_M and D_A those are used for learning a multi-label classifier f_r (*critic network*) and exploring the augmentation policy \mathcal{T} , respectively. The following loss function is employed to find the optimal augmentation policies,

$$\mathcal{T}_* = \operatorname{argmax}_{\mathcal{T}} \mathcal{R}(f_r | \mathcal{T}(D_A)) \quad (2)$$

where f_r is pre-trained on D_M . $\mathcal{T}(D_A)$ is the augmented datasets $\mathcal{T}(D_A) = \{\mathcal{T}(x) | x \in D_A\}$. \mathcal{T}_* minimizes the density gap of D_M and D_A from the perspective of enhancing the generalization ability of f_r to D_A .

Normally, the scales of $\mathcal{T}(D_A)$ is several times smaller than the original D_{train} , limiting the generalization the learnt \mathcal{T}_* . To this end, we propose to improve the density matching by enlarging the

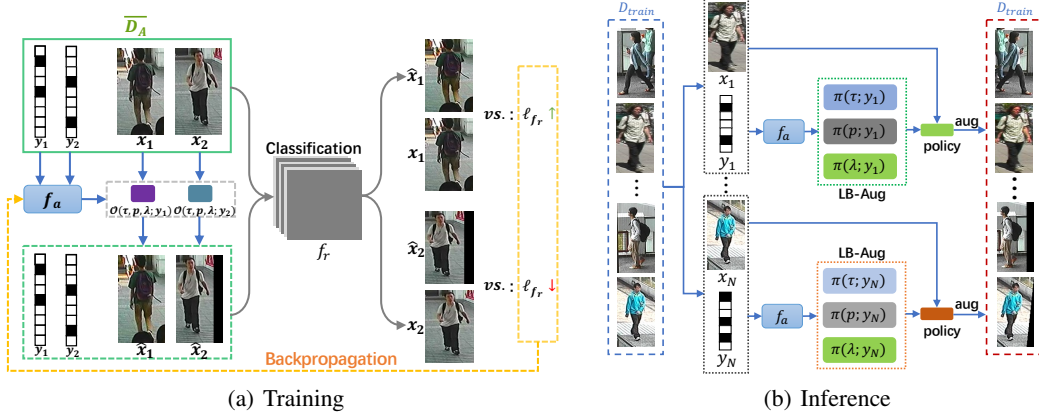


Figure 2: (a) The training of the actor network f_a . For each instance in \overline{D}_A , its corresponding critic network f_r evaluates the gain/drop of applying a testing augmentation policy on it. Then the comparison results are rewarded to f_a . In this way, f_a updates its parameters through backpropagation. (b) An example of augmenting Peta training dataset via LB-Aug. The actor network takes the multi-hot label y of each instance x as input, then predicts specific probability distributions of operation τ , calling probability p and magnitude λ , each of which is label-based. After that, the label-based policy is conducted to augment the input instance x .

training set of \mathcal{T} with full use of D_{train} . Considering the original training set D_{train} , the improved density matching uses K-fold stratified shuffling [15] to get K segmentations $\{S^{(1)}, \dots, S^{(K)}\}$, each $S^{(k)}$ consists of two datasets $D_M^{(k)}$ and $D_A^{(k)}$, where $D_{train} = D_M^{(k)} \cup D_A^{(k)}$. Following that, we first train a multi-label classifier $f_r^{(k)}$ on each $D_M^{(k)}$. Then, we get an unified evaluation set

$$\overline{D}_A = \bigcup_{k=1}^K D_A^{(k)} \quad (3)$$

Assuming an instance $x \in D_A^{(k)}$, the multi-label classifier $f_r^{(k)}$ trained on $D_M^{(k)}$ is thought as its corresponding critic network. Obviously, each instance in \overline{D}_A has at least one corresponding critics. We introduce the training of actor network taking \overline{D}_A as the training set, which is described next.

Given an instance (x_i, y_i) in \overline{D}_A , the searching of its optimal policy is based on Policy Gradient [8], which has two terms: 1) an actor network f_a predicts the optimal policy $\mathcal{O} = (\tau, p, \lambda, y_i)$ while taking label y_i as input. 2) the corresponding critic networks $\{f_r^{(k)} | x_i \in D_A^{(k)}, \forall k\}$ to reward \mathcal{O} , as illustrated in Figure 2(a). In detail, actor network f_a provides an triple probability distributions

$$(\pi(\tau; y_i), \pi(p; y_i), \pi(\lambda; y_i)) = f_a(y_i) \quad (4)$$

Here $\pi(\tau; y_i) \in \mathbb{R}^{C_\tau}$ is a vector that indicates the probability distribution of calling each operation. Each row of $\pi(p; y_i) \in \mathbb{R}^{C_\pi \times C_p}$ and $\pi(\lambda; y_i) \in \mathbb{R}^{C_\pi \times C_\lambda}$ presents the probability distributions of aforementioned discretized calling probabilities and magnitudes, respectively. During inference, a categorical distribution is conducted with $\pi(\tau; y_i)$ to sample an augmentation operation, for example τ_j . Its calling probability and magnitude are then sampled with probabilities $\pi_j(p; y_i)$ and $\pi_j(\lambda; y_i)$.

To maximize the gain of sub-policies, a form of difference loss is considered to train the actor network f_a :

$$\mathcal{L} = \frac{1}{N} \sum_{i=1}^N \mathbb{E}_{jkl} \log \pi(\tau_j, p_k, \lambda_l; y_i) \Delta \ell \quad (5)$$

For simplification, the calling probability and magnitude are considered independent from each other, so that the chain rule is available:

$$\pi(\tau_j, p_k, \lambda_l; y_i) = \pi(\tau_j; y_i) \pi_j(p_k; y_i) \pi_j(\lambda_l; y_i) \quad (6)$$

$\Delta\ell$ is the reward considered as the gain of classification loss from multi-label critic network $f_r^{(k)}$

$$\Delta\ell = \mathbb{E}_{x_i \in D_A^{(k)}} \left[\ell_{f_r^{(k)}}(x_i, y_i) - \ell_{f_r^{(k)}}(\hat{x}_i, y_i) \right] \quad (7)$$

$\ell_{f_r^{(k)}}$ is a binary cross entropy loss between the prediction of x_i and ground-truth label y_i . \hat{x}_i is the augmented counterpart of x_i and $\hat{x}_i = \tau_j(x_i; p_k, \lambda_l)$. Intuitively, the loss \mathcal{L} increases the probability of group (τ, p, λ) which leads to better performance gain, and vice versa.

3.2.2 Label-based Augmentation for Multi-label Classification

Figure 2(b) presents the usage of actor networks learned preliminarily. Taking the label y_i as input, a label-based augmentation policy is predicted for each instance $(x_i, y_i) \in D_{train}$ by the well-trained actor network f_a . It could remedy the distribution gap of original training set D_{train} and validation set D_{valid} more flexibly than label-agnostic ones. In this way, the proposed LB-Aug enhances the generalization of the final multi-label classifier f_c (having the same architecture as f_r by default).

A unique advantage of LB-Aug is that it is embedded with label-based information so that the augmentation of instances is not fixed globally but adaptive to each individual. In this way, it is superior to handle the severe problem faced by multi-label tasks that different labels are sensitive to different augmentations.

4 Experiments

Extensive experiments are first conducted to evaluate the effectiveness and superiority of the LB-Aug by comparing it with some baseline methods (Section 4.2) and previous SOTA approaches (Section 4.3), followed with a number of ablation studies showing how the method contributes to the performance gain of each label (Section 4.4.1) and how its performance is influenced by different settings on RL frameworks and the number of folds for density matching (Section 4.4.3 to 4.4.4).

4.1 Experimental Setup

Dataset and Evaluation Metrics We evaluate our method on three image/video datasets with standard evaluation protocols. For multi-label image classification task, we use Peta [7] and MS-COCO [16] datasets, report the standard attribute-wise mean accuracy (mA), overall accuracy (Accu), F1 for Peta and mAP, per-class F1 (CF1), overall F1 (OF1) for MS-COCO. For the multi-label video recognition experiment, we consider the widely used Charades [17] and only mAP is evaluated, following [3].

Peta is a large-scale pedestrian attributes dataset containing 19.0K images among which 9.5K is used for training, 1.9K for validation and 7.6K for model evaluation [18]. It has 61 binary attributes and 4 multi-class attributes. While, we only fetch 35 attributes whose positive proportions are larger than 5% for model analysis. *MS-COCO* is also a widely used image classification baseline. It contains about 82.1K images for training, 40.5K for validation and 40.7K for test. On average, each image has 2.9 labels from a set of 80 object labels. *Charades* has 157 action classes containing around 9.8K daily indoors activities videos, where 8.0K is for training and 1.8K for validation. Each video is labeled with 6.8 actions on average.

Augmentation Operations The search space consists of 16 operations (ShearX, ShearY, TranslateX, TranslateY, Rotate, AutoContrast, Invert, Equalize, Solarize, Posterize, Contrast, Color, Brightness, Sharpness, Cutout and Sample Pairing). The magnitude of each operation follows the default ranges in AutoAugment (AA) [4] and Fast AutoAugment (FAA) [5].

Architecture By default, our experiments use standard ResNet50, ResNet101 and Inception-V3 for image classification tasks, Inception-I3D and S3D for video recognition tasks. The outputs are activated by Sigmoid and learned by joint binary cross entropy loss. For actor networks, we concatenate three fully connected layers with Dropout rate 0.5 and ReLU superimposing.

Training Details The training of LB-Aug is boosted by the improved density matching (Section 3.2.1). Unless noted otherwise, we split training datasets into 8 folds with Stratified Shuffling [5], where 4/5 of original training set is segmented as D_M and the rest as D_A . For Peta and MS-COCO, we use SGD as optimizer with a mini-batch size of 80 and initial learning rate of 0.001. The weight

decay is 10^{-4} and momentum is 0.9. For Charades, each crop is randomly cropped into 224×224 from a 256×256 scaled video. Adam with initial learning rate 0.001 and weight decay 10^{-4} is used as optimizer for better convergence. The mini-batch size is 8 clips, while the accumulated gradient [19] of step 8 is utilized to stabilize the model training.

4.2 Comparisons with Baselines

The quantitative evaluation on multi-label image classification is shown in Table 1 and 2, and multi-label video recognition in Table 3. For each table, we compare the gain of Random policies (noted by ‘‘Baseline+Random’’), FAA, our LB-Aug_E (with fixed hyper-parameters) and LB-Aug_H (with trainable calling probabilities and magnitudes) over baseline models. In this paper we omit comparing our result with AA for two aspects: 1) AA [4] is computationally consuming and the training of augmentation policies takes thousands of GPU hours. 2) FAA is an accelerated alternative to AA with little performance gap, which is demonstrated in [5]. Additionally, the released experiments on FAA [5] is limited in single label tasks. For fair comparison on multi-label tasks, we conduct FAA with the released code of [5] and follow its best setting.

The training and testing protocols are kept the same for all methods except that the training of FAA follows Bayesian optimization [5].

Table 1: Performance comparison on Peta among baselines and LB-Aug.

Method	ResNet50			ResNet101			Inception-V3		
	mA	Accu	F1	mA	Accu	F1	mA	Accu	F1
Baseline [†]	84.9	78.1	85.5	85.4	78.9	85.8	86.0	79.6	86.5
Baseline+Random [‡]	85.2	78.5	85.2	85.6	79.0	86.0	86.2	79.7	86.5
FAA [5]	85.5	78.9	85.7	85.8	79.3	86.4	86.4	79.8	86.8
LB-Aug _E [*]	86.6	79.9	86.8	86.6	80.1	86.8	87.2	80.8	87.3
LB-Aug _H [*]	86.8	80.1	87.0	87.0	80.4	87.1	87.4	80.9	87.6

[†] : counterpart without additional augmentation from search space.

[‡] : counterpart with random policies from search space.

^{*} : counterpart with fixed calling probabilities 0.5 and magnitudes 1.

^{*} : counterpart with learnable calling probabilities and magnitudes.

Table 2: Comparisons between baselines and LB-Aug on MS-COCO.

Method	ResNet50			ResNet101			Inception-V3		
	mAP	CF1	OF1	mAP	CF1	OF1	mAP	CF1	OF1
Baseline	74.7	69.4	73.8	77.1	71.3	76.0	77.6	74.1	76.4
Baseline+Random	75.1	70.6	74.1	77.4	72.8	76.7	78.2	74.4	76.7
FAA	76.0	71.1	75.3	78.7	73.5	76.4	79.1	74.7	76.9
LB-Aug _E	77.1	72.3	76.2	79.7	74.5	77.5	80.2	75.9	77.8
LB-Aug _H	77.4	72.6	76.5	80.1	74.8	77.8	80.4	76.2	78.0

Table 3: Performance for multi-label video recognition on Charades.

Backbone	Baseline	Baseline+Random			FAA	LB-Aug
		$p^\dagger = 0.25$	$p = 0.75$	$p = 1$		
I3D	36.3	35.5	34.8	34.1	36.4	37.6
S3D	36.8	36.2	35.7	35.0	37.0	38.0

[†] : the magnitude of augmentation operations.

Multi-label Image Classification Table 1 and Table 2 show the comparison results with various augmentation methods and backbones: ResNet50, ResNet101 and Inception-V3. In this case, randomly chosen augmentation policies could lead to better generalization of all three backbones due to a suitable search space for these tasks, nevertheless the gains is relatively trivial. Compared with previous state-of-the-art FAA, our two counterparts LB-Aug_E and LB-Aug_H both provide

substantially improvement over all evaluation metrics. In particular, FAA and LB-Aug_H both adaptively learn the hyper-parameters, while with vital label information embedded, our LB-Aug_H leads to over 1.0% mA, 1.1% Accu and 0.7% F1 in Peta, as well as over 1.3% mA, 1.3% CF1 and 1.1% OF1 in MS-COCO.

Multi-label Video Recognition For the task of multi-label video recognition, we show the results on two backbone models: I3D and S3D in Table 3. The search space is inherited from Peta and MS-COCO, except that the videos are augmented frame by frame. Contrary to the results on Peta and MS-COCO, random augmentation policies drop over 0.8% mAP due to the amateurish search space for video tasks. While both FAA and our LB-Aug could still get gains over baseline. We notice that benefited from a fine-grained searching mechanism, our LB-Aug outperforms FAA by solid margins (37.6% vs. 36.4% for I3D, 38.0% vs. 37.0% for S3D).

4.3 Comparisons with State-of-the-arts

The proposed LB-Aug achieves two new SOTA performances on both Peta and MS-COCO with more strong backbone models. Table 4 presents the comparison results of LB-Aug against other SOTA methods on Peta. In comparison to the previous SOTA work GRL [20], our best model suggests up to 0.7% higher mA and 1.1% higher F1 while with the same backbone Inception-V3. In additional, GRL makes gains over backbone Inception-V3 by utilizing extra body region proposal and a Recurrent Neural Network (RNN), which enlarges the computation cost. Instead, the result of our proposed LB-Aug is achieved only taking backbone Inception-V3 as classifiers without other tricks on model design. On the experiments on MS-COCO, with the SOTA backbone model TResNet-L, our model achieves a 0.3% gain on mAP. Under the same experimental setting, the gain is up to 0.6%. Specifically, the gains on Peta and MS-COCO are both made by leveraging the label information for data augmentation without any extra modification on algorithm itself. We emphasize that our mechanism could be a more naive way to get bonus from other state-of-the-art works.

Table 4: Comparing LB-Aug against other SOTA methods on Peta.

Methods	Backbone	Pretrain	mA	Accu	F1
JRL [21]	AlexNet	ImageNet	85.7	–	85.4
DeepMar [22]	CaffeNet	ImageNet	82.9	75.1	83.4
DeepMar [†] [22]	Inception-V3	ImageNet	81.5	–	85.7
VeSPA [23]	GoogleNet	ImageNet	83.5	77.7	85.5
WPAL [24]	GoogleNet	ImageNet	85.5	77.0	84.9
PGDM [25]	CaffeNet	ImageNet	83.0	78.1	85.8
ALM [18]	BN-Inception	–	86.3	79.5	86.9
GRL [20]	Inception-V3	ImageNet	86.7	–	86.5
FAA [5]	Inception-V3	ImageNet	86.4	79.8	86.8
LB-Aug _H	BN-Inception	ImageNet	86.7	80.1	87.2
LB-Aug _H	Inception-V3	ImageNet	87.4	80.9	87.6

[†] : reported by [20].

4.4 Ablation Studies

4.4.1 Label-wise Performance

Figure 3 shows the performance bonus of FAA and LB-Aug per label. FAA gets an mA bonus of 0.6% over baseline while benefited from learning better augmentation operations and hyper-parameters. However, compared to Baseline, its gain of overall mA mainly sources from enhancing the model performance on labels with more positive cases. As demonstrated in Table 3, it even drops its mA on labels with no sufficient positive rate. The intrinsic reason is that FAA is label-agnostic, meaning that it has to provide a compromised policy for better overall mA. Leveraged by more fine-grained and label-based search mechanism, our LB-Aug gets competitive performance against FAA on labels with large positive cases, while still keep performance gain over labels with small positive rate.

Table 5: Experimental comparison of SOTA methods on MS-COCO.

Methods	Backbone	Pretrain	mAP	CF1	OF1
SRN [26]	ResNet101	ImageNet	77.1	71.2	75.8
Multi-Evidence [27]	ResNet101	ImageNet	—	74.9	78.4
CADM [28]	ResNet101	ImageNet	82.3	77.0	79.6
ML-GCN [29]	ResNet101	ImageNet	83.0	78.0	80.3
KSSNet [3]	ResNet101	ImageNet	83.7	77.2	81.5
MS-CMA [30]	ResNet101	—	83.8	78.4	81.0
ASL [31]	TResNet-L	ImageNet	86.6 (86.4*)	81.4 (81.1*)	81.8 (81.6*)
ASL [31] [†]	TResNet-L	ImageNet	88.4 (88.1*)	— (81.6*)	— (82.3*)
LB-Aug _H [‡]	TResNet-L	ImageNet	86.9	81.6	81.9
LB-Aug _H [‡]	TResNet-L	ImageNet	88.7	82.3	82.7

* : our implemented results with the released code of [31].

† : input resolution is enlarged to 640 × 640

‡ : conducted following the released code of ASL [31]

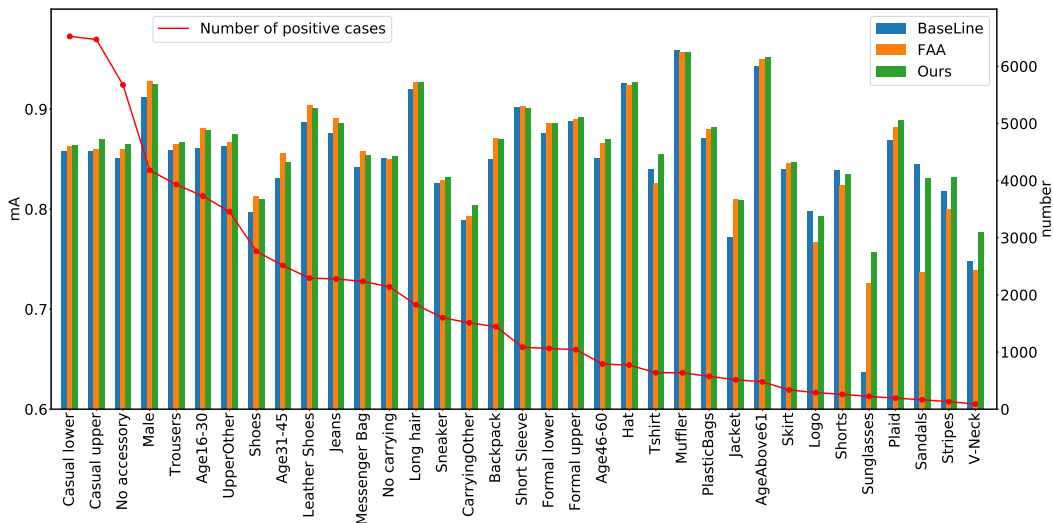


Figure 3: The mA histogram and positive case number of each label on Baseline ResNet50, FAA and LB-Aug.

4.4.2 Generalization to Other Models

We also show that a well trained policies from specific critic models can generalize to other models. Table 6 compares the evaluation results of ResNet101 and Inception-V3 with a fixed policy which is learned from taking critic network as ResNet50. It is shown that a well trained policy consistently improves the performance of other models by negligible margin with retrained ones.

Table 6: Comparing the mAP of fixed and retrained policy counterparts. The fixed policy is learned with critic model of ResNet50. The value in parentheses denotes the gain/drop over Table 1.

Method	ResNet101			Inception-V3		
	mA	Accu	F1	mA	Accu	F1
LB-Aug _E	86.6 (+0)	80.0 (-0.1)	86.6 (-0.2)	87.4 (+0.2)	80.9 (+0.1)	87.3 (+0)
LB-Aug _H	86.9 (-0.1)	80.3 (-0.1)	87.0 (-0.1)	87.5 (+0.1)	80.9 (+0)	87.5 (-0.1)

Table 7: Quantitative results on Peta of different reinforcement learning framework. All counterparts are based on ResNet50.

Framework	mA	Accu	F1
Policy Gradient [8]	86.8	80.1	87.0
DPG [32]	86.7	80.0	87.0
AC [33]	86.8	80.0	86.9
DQN [34]	86.2	79.6	86.7

4.4.3 Reinforcement Learning Framework

As we know, reinforcement learning suffers from the problem of convergence and sub-optimization, therefore different optimizers seems to have influence on the performance of LB-Aug. In order to analyze this influence, we conduct ablation study on the training framework of actor network on Peta dataset. Policy Gradient is used as the final reinforcement learning methods. For comparison, we also implements LB-Aug trained with AC [33], DPG [34] and DQN [32]. The LB-Aug is conducted as LB-Aug_E for simplification. As shown in Table 7, Policy Gradient, DPG and AC has comparable performance, while DQN acts worse on all three evaluation metrics. In summary, directly predicting the policies (the former three) instead of choosing one policy according to the overall rewards (DQN) is more effective to the task searching label-based augmentation policies.

4.4.4 Number of Folds

We conduct K-fold stratified shuffling to split the origin training dataset into two segmentations, D_M for training critic networks and D_A to train the actor network. Finally, with label-based augmentation policies predicted by the actor network, a new multi-label classifier which has the same frameworks as critic but different weight parameters will be trained. As the actor network is trained on the union of K splitted D_A (Eqn. 3), the number K determines the scale of training set $\overline{D_A}$ of the actor. Figure 4 illustrates the results on Peta and MS-COCO of K from 1 to 12.

In total, the performance is monotonically improved when we enlarge the numbers of folds. The curves in Figure 4 indicates two terms of gains: 1) The case where the scale of K is relatively small (less than 6 in Figure 4). Noting that the D_A is segmented with $1/5$ samples of original training set D_{train} . In this case, bigger K brings more training samples for the actor network, promoting better generalization. 2) The case where the scale of K is relatively large (larger than 6 in Figure 4). In this case, bigger K no longer produces larger training set because $\overline{D_A} \approx D_{train}$. Nevertheless, the instances in $\overline{D_A}$ tend to have more corresponding critic networks, such that the reward of a policy on these instances could be more solid for the actor network training. In summary, using additional folds could monotonically boost the performance.

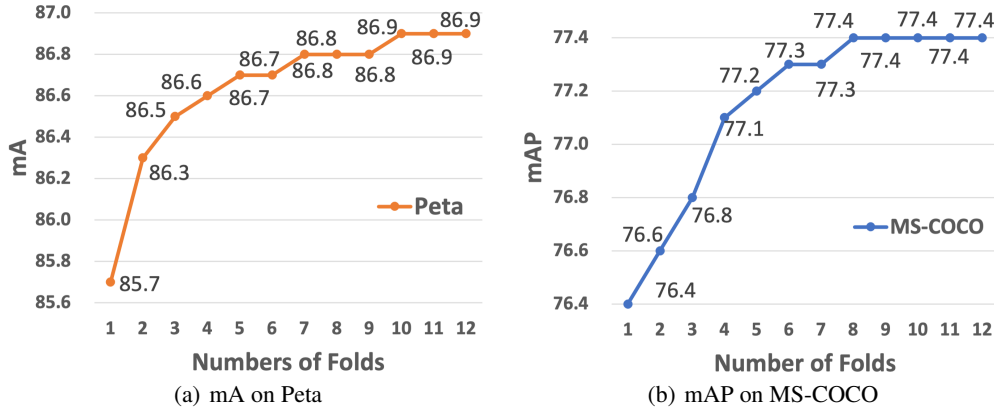


Figure 4: Performance curve on fold numbers K .

5 Conclusion

In this paper, we propose a novel label-based autoaugmentation method for multi-label image/video classification tasks. Benefitting from data augmentation policies fine-grained by considering instance labels, our method outperforms existing SOTA augmentation approaches by large margins in Peta, MS-COCO and Charades benchmarks. Extensive ablation study shows that the proposed LB-Aug method is compatible to most widely used architectures, with all of which the LB-Aug achieves the SOTA performance. Moreover, the method can be further extended to other multi-label style tasks such as ReID, Semantic Segmentation, and even unsupervised learning tasks wherever fine-grained information and rewards for actor network learning are available.

References

- [1] Esteban Real, Alok Aggarwal, Yanping Huang, and Quoc V Le. Regularized evolution for image classifier architecture search. In *Proceedings of the aaai conference on artificial intelligence*, volume 33, pages 4780–4789, 2019.
- [2] Fuxiang Huang, Lei Zhang, Yang Yang, and Xichuan Zhou. Probability weighted compact feature for domain adaptive retrieval. In *Proceedings of the IEEE/CVF Conference on Computer Vision and Pattern Recognition*, pages 9582–9591, 2020.
- [3] Ya Wang, Dongliang He, Fu Li, Xiang Long, Zhichao Zhou, Jinwen Ma, and Shilei Wen. Multi-label classification with label graph superimposing. In *Proceedings of the AAAI Conference on Artificial Intelligence*, volume 34, pages 12265–12272, 2020.
- [4] Ekin D Cubuk, Barret Zoph, Dandelion Mane, Vijay Vasudevan, and Quoc V Le. Autoaugment: Learning augmentation strategies from data. In *Proceedings of the IEEE conference on computer vision and pattern recognition*, pages 113–123, 2019.
- [5] Sungbin Lim, Ildoo Kim, Taesup Kim, Chiheon Kim, and Sungwoong Kim. Fast autoaugment. In *Advances in Neural Information Processing Systems*, pages 6665–6675, 2019.
- [6] Xinyu Zhang, Qiang Wang, Jian Zhang, and Zhao Zhong. Adversarial autoaugment. *arXiv preprint arXiv:1912.11188*, 2019.
- [7] Yubin Deng, Ping Luo, Chen Change Loy, and Xiaoou Tang. Pedestrian attribute recognition at far distance. In *Proceedings of the 22nd ACM international conference on Multimedia*, pages 789–792, 2014.
- [8] Richard S Sutton, David A McAllester, Satinder P Singh, and Yishay Mansour. Policy gradient methods for reinforcement learning with function approximation. In *Advances in neural information processing systems*, pages 1057–1063, 2000.
- [9] Jie Hu, Li Shen, and Gang Sun. Squeeze-and-excitation networks. In *Proceedings of the IEEE conference on computer vision and pattern recognition*, pages 7132–7141, 2018.
- [10] Christoph Feichtenhofer, Haoqi Fan, Jitendra Malik, and Kaiming He. Slowfast networks for video recognition. In *Proceedings of the IEEE international conference on computer vision*, pages 6202–6211, 2019.
- [11] Terrance DeVries and Graham W Taylor. Improved regularization of convolutional neural networks with cutout. *arXiv preprint arXiv:1708.04552*, 2017.
- [12] Cecilia Summers and Michael J Dinneen. Improved mixed-example data augmentation. In *2019 IEEE Winter Conference on Applications of Computer Vision (WACV)*, pages 1262–1270. IEEE, 2019.
- [13] John Schulman, Filip Wolski, Prafulla Dhariwal, Alec Radford, and Oleg Klimov. Proximal policy optimization algorithms. *arXiv preprint arXiv:1707.06347*, 2017.
- [14] Daniel Ho, Eric Liang, Xi Chen, Ion Stoica, and Pieter Abbeel. Population based augmentation: Efficient learning of augmentation policy schedules. In *International Conference on Machine Learning*, pages 2731–2741. PMLR, 2019.
- [15] Mohammad Shahrokh Esfahani and Edward R Dougherty. Effect of separate sampling on classification accuracy. *Bioinformatics*, 30(2):242–250, 2014.

- [16] Tsung-Yi Lin, Michael Maire, Serge Belongie, James Hays, Pietro Perona, Deva Ramanan, Piotr Dollár, and C Lawrence Zitnick. Microsoft coco: Common objects in context. In *European conference on computer vision*, pages 740–755. Springer, 2014.
- [17] Gunnar A. Sigurdsson, Gül Varol, Xiaolong Wang, Ali Farhadi, Ivan Laptev, and Abhinav Gupta. Hollywood in homes: Crowdsourcing data collection for activity understanding. In *European Conference on Computer Vision*, 2016.
- [18] Chufeng Tang, Lu Sheng, Zhaoxiang Zhang, and Xiaolin Hu. Improving pedestrian attribute recognition with weakly-supervised multi-scale attribute-specific localization. In *Proceedings of the IEEE International Conference on Computer Vision*, pages 4997–5006, 2019.
- [19] Yujun Lin, Song Han, Huizi Mao, Yu Wang, and William J Dally. Deep gradient compression: Reducing the communication bandwidth for distributed training. *arXiv preprint arXiv:1712.01887*, 2017.
- [20] Xin Zhao, Liufang Sang, Guiguang Ding, Yuchen Guo, and Xiaoming Jin. Grouping attribute recognition for pedestrian with joint recurrent learning. In *IJCAI*, pages 3177–3183, 2018.
- [21] Jingya Wang, Xiatian Zhu, Shaogang Gong, and Wei Li. Attribute recognition by joint recurrent learning of context and correlation. In *Proceedings of the IEEE International Conference on Computer Vision*, pages 531–540, 2017.
- [22] Dangwei Li, Xiaotang Chen, and Kaiqi Huang. Multi-attribute learning for pedestrian attribute recognition in surveillance scenarios. In *2015 3rd IAPR Asian Conference on Pattern Recognition (ACPR)*, pages 111–115. IEEE, 2015.
- [23] M Saquib Sarfraz, Arne Schumann, Yan Wang, and Rainer Stiefelhagen. Deep view-sensitive pedestrian attribute inference in an end-to-end model. *arXiv preprint arXiv:1707.06089*, 2017.
- [24] Yang Zhou, Kai Yu, Biao Leng, Zhang Zhang, Dangwei Li, Kaiqi Huang, Bailan Feng, Chunfeng Yao, et al. Weakly-supervised learning of mid-level features for pedestrian attribute recognition and localization. 2017.
- [25] Li Dangwei, Chen Xiaotang, Zhang Zhang, Huang Kaiqi, et al. Pose guided deep model for pedestrian attribute recognition in surveillance scenarios. 2018.
- [26] Feng Zhu, Hongsheng Li, Wanli Ouyang, Nenghai Yu, and Xiaogang Wang. Learning spatial regularization with image-level supervisions for multi-label image classification. In *Proceedings of the IEEE Conference on Computer Vision and Pattern Recognition*, pages 5513–5522, 2017.
- [27] Weifeng Ge, Sibe Yang, and Yizhou Yu. Multi-evidence filtering and fusion for multi-label classification, object detection and semantic segmentation based on weakly supervised learning. In *Proceedings of the IEEE Conference on Computer Vision and Pattern Recognition*, pages 1277–1286, 2018.
- [28] Zhao-Min Chen, Xiu-Shen Wei, Xin Jin, and Yanwen Guo. Multi-label image recognition with joint class-aware map disentangling and label correlation embedding. In *2019 IEEE International Conference on Multimedia and Expo (ICME)*, pages 622–627. IEEE, 2019.
- [29] Zhao-Min Chen, Xiu-Shen Wei, Peng Wang, and Yanwen Guo. Multi-label image recognition with graph convolutional networks. In *Proceedings of the IEEE/CVF Conference on Computer Vision and Pattern Recognition*, pages 5177–5186, 2019.
- [30] Renchun You, Zhiyao Guo, Lei Cui, Xiang Long, Yingze Bao, and Shilei Wen. Cross-modality attention with semantic graph embedding for multi-label classification. In *Proceedings of the AAAI Conference on Artificial Intelligence*, volume 34, pages 12709–12716, 2020.
- [31] Emanuel Ben-Baruch, Tal Ridnik, Nadav Zamir, Asaf Noy, Itamar Friedman, Matan Protter, and Lihi Zelnik-Manor. Asymmetric loss for multi-label classification. *arXiv preprint arXiv:2009.14119*, 2020.
- [32] Volodymyr Mnih, Koray Kavukcuoglu, David Silver, Alex Graves, Ioannis Antonoglou, Daan Wierstra, and Martin Riedmiller. Playing atari with deep reinforcement learning. *arXiv preprint arXiv:1312.5602*, 2013.
- [33] Vijay R Konda and John N Tsitsiklis. Actor-critic algorithms. In *Advances in neural information processing systems*, pages 1008–1014, 2000.
- [34] David Silver, Guy Lever, Nicolas Heess, Thomas Degris, Daan Wierstra, and Martin Riedmiller. Deterministic policy gradient algorithms. 2014.

Supplementary Materials

A Supplementary of Figure 1(a)

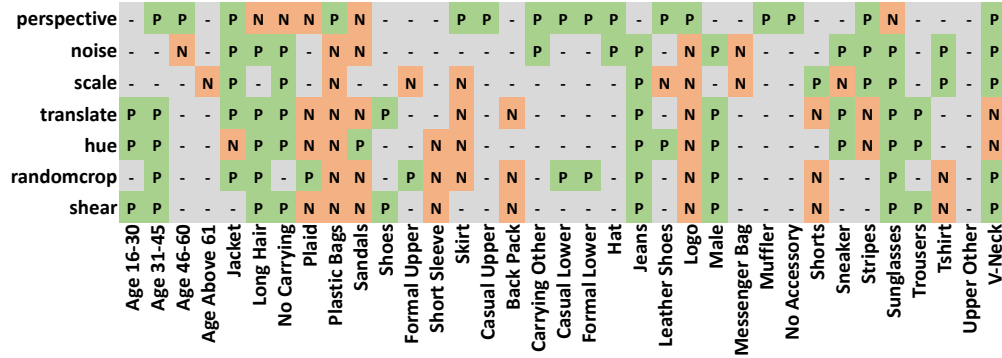


Figure 5: The gain/drop of augmentations on all labels of Peta. “P” indicates positive effects on the classification. “N” presents the effects are negative and “-” means inconspicuous influences.

B Depth of Actor Network

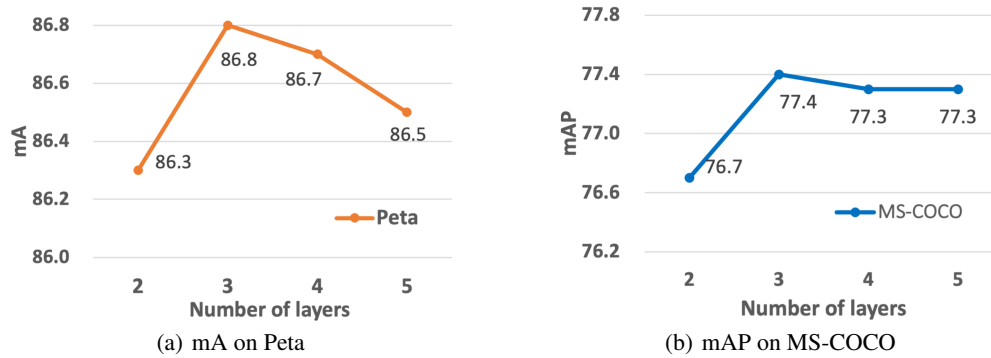


Figure 6: The mA results on Peta and mAP results on MS-COCO. Each fully connected layer is followed by an ReLU and Dropout whose drop rate is 0.5.

The actor network of our LB-Aug is constructed with fully connected layers which are equipped with ReLU to make a non-linear transformation and Dropout to overcome the overfitting problem. Figure 6 shows how the depth of the actor network (varying from 2 to 5) influences its performance. We can see that the depth of three works significantly better than depth 2, while as the network goes deeper, its performance on MS-COCO decreases slightly, while drops more distinctly on Peta. We think the reason why the depth of 2 has worse performance than that of the depth of 3 is the limitation of network capacity. Meanwhile, the performance decreases of those networks deeper than 3 are well possible caused by the “overfitting” problem, as the data augmentation policy learning task whose input is a multi-hot vector (whose dimension equals to the number of labels: 35 on Peta and 80 on MS-COCO) and output is the probabilities of taking each augmentation operation (whose dimension equals to the number of possible data augmentation operations: 16 in this paper), are relatively simpler than those complicated classification tasks such as the multi-label benchmarks used in this paper.